

The turbulent flow between two rotating stirrers : similitude laws and transitions for the driving torques.

Olivier Cadot¹ and Olivier Le Maître²

¹*Unité de Mécanique de l'Ecole Nationale Supérieure de Techniques Avancées,
Chemin de la Hunière, 91 761 Palaiseau Cedex, France.
corresponding author : cadot@ensta.fr*

²*Laboratoire de Mécanique et d'Energétique, Université d'Evry,
40 rue du Pelvoux, 91020 Evry Cedex, France.*

Instantaneous torques driving the turbulent flow between two rotating disks equipped with blades and enclosed in a fixed cylindrical cell are measured. The flow is studied varying the Reynolds number for different angular velocity ratios S of the disks in order to extract similitude laws. It is shown that the mean torques driving the disks do not depend on the viscosity whatever the rotation angular velocity ratio $-1.33 < S < -0.69$. As far as the viscosity dependance is not too large, the torques obey a similitude law so the study can be restricted to the study of the flow in the range $S = [-1; +1]$. Global transitions are observed versus S , shown of by abrupt changes in both the means and the fluctuations of the torques. A transition occuring at $S = -0.69$ is clearly identified corresponding to the well known one to two cells transition previously observed for smooth disks and similarities between smooth and bladed disks are discussed. The torque measurements also suggest other transitions in the co-rotating regime ($S > 0$).

Keywords : Turbulent torque, Similarities, Transitions.

PACS numbers : 47.27.-i, 05.40.-a

1. Introduction

The flow between two rotating disks is of practical importance in many industrial flows. On the fundamental point of view, this flow is very complicated, and depends drastically on the boundary conditions [1]. Simple questions as : does the flow still rotate for very high Reynolds numbers in the counter rotation regime? has standed as a major problem [2]. Most studies, theoretical, experimental or numerical are devoted to the problem initially set by von-Karman : the flow between two infinite smooth disks. When the disks are not infinite, the condition imposes severe constraints on the flow leading to very different solutions [3]. In the case of smooth disks, it is established that within the case of the counter-rotating regime, there is a transition for a given Eckmann number and rotation velocity ratio from one cell to two cells structure (primary reported by Lugt & Haussling [4], and checked numerically by Dijkstra & Heijst [3]). This transition corresponds to the emergence of a detached shear layer on the disk having the slower angular velocity.

The flow considered in this paper, though concerning finite disks, differs from the previous studies because the disks are equipped with blades pushing the flow (see figure 1). This type of flow, and especially in the exact counter rotating regime is now extensively used in the aim of studying fundamental aspect of developed turbulence. The reason comes from appreciable advantages due to the closed flow (compared to classical open flows) that has been successfully used for comprehension of turbulence as for instance : dynamical structures observations [5] and characterizations [6], global power fluctuations [7,8], drag reduction by polymer additives [9], passive scalar intermittency [10], particule accelerations [11] and magneto-hydrodynamics turbulence [12]. Particularly, this flow was found to follow the Kolmogorov K41 scaling for the global mean dissipation [13,14] (no viscosity dependency) for the exact counter-rotating regime.

Our idea is to characterize the flow produced in this geometry (with blades) for different angular velocities of both disks (differential rotation) and to compare to previous results found in the literature about smooth disks. Only few articles are devoted to the characterization of the global flow properties in this geometry. To our knowledge, Marié *et al.* [15] characterized the mean kinetic momentum by means of LDV measurements in the exact counter rotating regime. Very recently, Ravelet [16] explored the flow in the counter-rotating regime ($S \leq 0$) by means of global torques PIV velocity measurements. It is found a global transition from a one cell to a two cells for $S = -0.78$ similar to those observed for smooth disks. In the work of Ravelet *et al.* [17], this global transition is found to be spontaneous (or discontinuous) for the very specific case of curved blades and for the exact counter-rotating regime ($S = -1$). However the appearance of this discontinuity is related to the curvature of the blades and do not concerns our study since the blades pushing the flow in our geometry are straight .

The characterization is obtained by mean of instantaneous torque measurement on both disks. We are interested in the evolution of the mean torques and their fluctuations (*rms* value) for both disks versus the angular rotation ratio. The present work is organized as follow; the experimental set up is first presented in sec. 2 and concerns the experimental geometry, torque measurements and flow visualization. Section 3 is a preliminary and will recall the momentum budget equation for this geometry as well as some symmetry properties of the flow forcing. The results will be presented in section 4 and discussed in three parts in section 5. These three discussions are about similtude laws, the one to two cells transition for the counter rotating regime and the dependence of the torque fluctuations on the angular velocity ratio.

2. Experimental set-up

2.1 Experimental Cell

Titon & Cadot [14] have previously described this experimental cell in detail. The turbulence is generated in a closed cylindrical cell ($V=11$ liters) between two rotating stirrers (disk with blades) of radius $R=8.75$ cm spaced a distance $H=320$ mm apart (see figure1 for specific sizes). Two DC servomotors regulated by servo amplifier (from Parvex) independently drive each stirrer. The motors are configured to keep the disks rotating at constant angular velocity Ω , independently of the torque exerted by the turbulence on the disks. This is done by using a tachymetry feedback loop, a regulation system that adapts the torque delivered by the motors to maintain the imposed angular velocity. The time response of the control loop is 0.05s, implying a high-frequency cut-off of 20 Hz (see [14] for further details). For lower frequencies, the image of the electric current measured as a voltage output of the regulation gives an instantaneous measurement of the torque. The electric current is directly proportional to the torque following the Laplace law. 1 volt of torque signal output corresponds to 0.52 N.m. In the following the torques are presented in arbitrary units for which 1 U.A. of torque = 0.52 N.m, and the frequencies of rotation are in Hz. The instantaneous torque delivered by each DC servomotor, $\Gamma_B^M(t)$ and $\Gamma_T^M(t)$ are analyzed with a data acquisition board and LABVIEW software.

For the present experiments the working fluid is always water and only the angular velocities on both disks are varied. The Reynolds numbers reaches at maximum, a magnitude

$$\text{of : } \text{Re} = \frac{|\Omega_B - \Omega_T| R^2}{2\nu_{\text{water}}} \leq 200\,000$$

2.2 Instantaneous turbulent torque measurements

The drag torque $\Gamma_i(t)$ due to the fluid flow on the disk i ($i=B$ or T) rotating at the angular velocity Ω_i is computed by subtracting to the motor's torque $\Gamma_i^M(t)$, the torque due to the torques of mechanical friction losses Γ_i^S which were measured independently in the empty cell (full of air). We have:

$$\Gamma_i(t) = \Gamma_i^M(t) - \Gamma_i^S(\Omega_i),$$

2.3 Flow visualization

Visualization is realized by seeding the water with particles (PVC powder). Their averaged diameter is 150 microns and their density $d=1.35$. Since their density is larger than that of water the particles are also used as indicators of the pressure field in the cell. The crossed flow (corresponding to the figure 1 view) is video taped in a light sheet produced by a 4 Watt Argon laser. The shutter of the camera is set to $1/6s$ and the image rate is $1/50s$ (each frame results from an integration of the flow during a $1/6s$ time duration sliding window). The particles appear white on a black background, they mainly follow the velocity field escaping the large coherent low-pressure region because of their higher density than water.

3. Preliminary

3.1 Preliminary: momentum budget equation

The total flow of volume V is enclosed by a fixed cylinder of surface Σ_W and two rotating disks of surface Σ_B and Σ_T (see figure 1). Let $\Sigma = \Sigma_W + \Sigma_B + \Sigma_T$ denote the total surface.

The budget equation for the momentum taken from the symmetry axis (Δ) (see figure 1) expressed in cylindrical coordinates system reads :

$$\frac{\partial}{\partial t} \iiint_V \vec{r} \wedge \rho \vec{u} d\tau = - \iint_{\Sigma} (\vec{r} \wedge \rho \vec{u}) (\vec{u} - \vec{u}_s) \cdot \vec{n} dS + \iiint_V \vec{r} \wedge \rho \vec{g} d\tau + \iint_{\Sigma} (\vec{r} \wedge \underline{\underline{\sigma}} \cdot \vec{n}) dS, \text{ eq. 1}$$

where \vec{n} is the unit vector, normal to the surface S and pointing outward the fluid volume, \vec{u} the local velocity of the flow, \vec{u}_s the local velocity of the solid wall, ρ the fluid density, \vec{g} the gravity and $\underline{\underline{\sigma}}$ the total stress tensor. The left-hand-side is the rate of change in the total kinetic momentum. The first term of the right hand side is the flux of kinetic momentum through the total surface which is zero since the surfaces are non-porous implying $\vec{u} - \vec{u}_s = \vec{0}$. The second contribution is the external volume force momentum, only due to gravity in our case, which is zero since the gravity is paralell to the axis (Δ). The third contribution is the momentum of any surface forces applied on the surface Σ . Since the total surface basically decomposed itself into three surfaces (see figure 1) : this last term involves three contributions:

$$\iint_{\Sigma} (\vec{r} \wedge \underline{\underline{\sigma}} \cdot \vec{n}) dS = \Gamma_B + \Gamma_T + \Gamma_w, \text{ eq. 2}$$

Γ_B is the torque exerted on the bottom disk, Γ_T the torque exerted on the top disk and Γ_w is the torque exerted in the inner wall of the fixed cylinder. The budget equation for the kinetic momentum thus becomes :

$$\frac{\partial}{\partial t} \iiint_V \vec{r} \wedge \rho \vec{u} d\tau = \Gamma_B + \Gamma_T + \Gamma_w \text{ eq. 3}$$

By taking the time average of equation eq.3, the left-hand-side term becomes zero for stationary turbulence which leads to the simple relationship :

$$\langle \Gamma_B \rangle + \langle \Gamma_T \rangle + \langle \Gamma_w \rangle = 0 \text{ eq. 4}$$

The top and bottom time-averaged torques are strongly correlated depending on the torque exerted on the inner wall of the cylinder.

3.2 Symmetries

There are two symmetries of interest in this study. The first is in respect to the rotation direction (that we will refer as the *rotation direction symmetry*) and the second to the top and bottom exchange (that we will refer as the *inversion symmetry*).

The rotation direction symmetry is expressed as :

$$\begin{aligned}\Gamma_B(f_B = f_0; f_T = f) &= -\Gamma_B(f_B = -f_0; f_T = -f) , \\ \Gamma_T(f_B = f_0; f_T = f) &= -\Gamma_T(f_B = -f_0; f_T = -f) \quad \mathbf{eq. 5}\end{aligned}$$

and the inversion symmetry is expressed as :

$$\Gamma_B(f_B = f_0; f_T = f) = \Gamma_T(f_B = f; f_T = f_0) , \quad \mathbf{eq. 6}$$

4. Results

4.1 Turbulent torques over the disks vs. the rotation frequency ratio.

A typical experiment consists in a series of measurements that we call a run (see table 1). For a run, we set the rotation frequency of one of the disks to f_0 and vary the other one with a rotation frequency f . When a stationary regime of differential rotation is reached, we measure the time averaged torque of the bottom disk $\langle \Gamma_B \rangle$, and the top disk $\langle \Gamma_T \rangle$. The typical fluctuations of the torques are measured as the root mean square torques of both forcing devices, we denote them by $\delta \Gamma_T$ for the top disk and $\delta \Gamma_B$ for the bottom disk:

$$\delta\Gamma_T = \sqrt{\langle\Gamma_T^2\rangle - \langle\Gamma_T\rangle^2} \text{ and } \delta\Gamma_B = \sqrt{\langle\Gamma_B^2\rangle - \langle\Gamma_B\rangle^2}$$

The time duration on which the averaging are performed is long enough (typically 1 to 2 minutes depending on the rotation frequencies) to insure a good statistical convergence of the torque fluctuations. The measurements are repeated for different values (about 110 values) of f in the range $-2f_0$ and $+2f_0$. We performed three experimental runs (see Table 1); run #1 and run #2 have an identical fixed rotation frequency f_0 , but it is imposed by the bottom disk in run #1 while it is imposed by the top disk in run #2. In run #3, like in run #1, the fixed rotation frequency is imposed by the bottom disks but with a smaller magnitude. The results are displayed versus the rotation ratios either defined as: $S = \frac{f}{f_0}$ or $1/S = \frac{f_0}{f}$, where f_0 always refers to the fixed frequency and f to the variable frequency of the run. Table 1 lists the variations of both quantities for the three experimental runs.

In figure 2(a) and (b), we reported respectively the mean and the fluctuating torques of the top and bottom forcing devices as the function of $S = \frac{f}{f_0}$. The torques are divided by the square of the constant frequency rotation, f_0 that defines a "dimensionless torque" with respect to the only variable quantities of the experiments, say the frequency rotations. However it could be useful for comparison with other works to introduce the dimensionless κ torque defined as $\Gamma = \kappa\rho\Omega^2 R^5$. The conversion from our arbitrary "dimensionless torque" presented in our figures (2, 3, 4) and κ is : $\kappa=2.81* 1 A.U. \text{ of } \Gamma/f^2$.

The inversion symmetry (eq. 6) of the apparatus is very well checked in figure 2(a) for the mean torque of both disks where $\langle\Gamma_B\rangle/f_B^2$ [Resp. $\langle\Gamma_T\rangle/f_T^2$] measured in Run#1 is equal to $\langle\Gamma_T\rangle/f_B^2$ [Resp. $\langle\Gamma_B\rangle/f_T^2$] measured in Run#2. Moreover, the measurements of Run#3

performed at a lower fixed rotation frequency collapse on the data performed at higher fixed rotation frequency f_0 (Run#1 and #2). Hence the result suggests that the "non-dimensional" torques as defined above only depend on the rotation frequency ratio.

In the case of the torques fluctuation shown in figure 2(b), the measurements are slightly more scattered, but the symmetry is also globally checked satisfactorily when comparing run #1 and #2. It can be concluded that both motors are then very similar and the experimental set-up provides quite accurate measurements of the instantaneous torques. Data of run #3 confirm the measurements performed at larger fixed rotation frequency (Run#1 and #2) only for the measured at bottom disk (whose rotation frequency is fixed to $f_0=4.5\text{Hz}$). Actually, for the top disk, the fluctuations contains a sinusoidal signal having the rotation frequency. The origin of this spurious signal is not hydrodynamics but comes from a small defect of the DC motor. In run#3, where the rotational frequency of the disk is low, this signal dominates the fluctuations around $S=-0.5$ and $S=1$. Hence, except this experimental defect, measurements provide that the torque fluctuations when non-dimensionalized by the square of the rotation frequency seems to depend only on the rotation frequency ratio.

This similitude behavior allows for a simpler representation of the data. Actually, the scaling law as the square of the rotation frequency together with the inversion symmetry imply that the measurements of both torques for $|S| \geq 1$ are the same measurements that those obtained for $|S| \leq 1$ whatever the rotation frequencies (or the Reynolds number of the flow). This is reasonably checked on the next figure 3 where plotted are the non-dimensional torques, $\Gamma'_B = \frac{\Gamma_B}{f_B^2}$ and $\Gamma'_T = \frac{\Gamma_T}{f_T^2}$ versus S (for $|S| \leq 1$) measured in run#1 and their symmetric counterpart (in respect to eq.5 and eq.6), $\text{sign}(S) \frac{\Gamma_B}{f_T^2}$ and $\text{sign}(S) \frac{\Gamma_T}{f_B^2}$ versus $1/S$ (for $|S| \geq 1$).

We can see on the figure 3(a) that the mean torques collapse satisfactorily. The same behavior is also observed for the torque fluctuations in figure 3(b).

4.2 Torque exerted on the inner wall cell.

The time averaged torque exerted on the inner wall of the cylindrical cell is computed from equation eq.4. The continuous lines in figure 4 shows the non-dimensional wall torque defined as $\langle \Gamma_w \rangle / f_B^2$ for run#1 and run #3 versus $S \in [-1,1]$. The wall torque is zero for $S=-1$ as expected from the experiment symmetries. The measurements for $S \leq -1$ and $S \geq 1$ correspond to the crosses and are plotted in the range S (or $1/S$) $\in [-1,1]$ using the symmetries (eq.5 and eq.6). Two distinct scaling regims can be distinguished for the ranges $-1 < S(1/S) < -0.67$ and $-0.67 < S(1/S) < 1$. In the range $-1 < S(1/S) < -0.67$, the curves collapse satisfactorily showing that in a range around $S=-1$, approximately : $-1.33 < S < -0.67$, the wall torque does not depend on viscosity. On the contrary, in the range $-0.67 < S(1/S) < 1$, the curves clearly do not collapse, indicating that the averaged wall torque does not scale with the rotational frequencies rotation only but also on the Reynolds number.

4.3 Visualization of the flow as a function of S.

We have so far quantified the torque's magnitudes, symetries and scaling, we now turn to the complex structure of the torques evolution with the frequency ratio. Our idea is to understand the torque behaviour with the help of the global time averaged flow visualization. We restrict the study between $-1 < S < +1$ only (this restriction is justified because of the symmetries and the scaling laws properties displayed in figure 3). In figures 5 and 6 the frequency of the bottom disk is set to 4.5Hz.

We first focus on the counter-rotating regime. Figure 5 shows the cross-flow for 4 negative values of S . The first picture in figure 5 shows the exact counter-rotating regime $S=-1$. The time averaged cross-flow consists in a cell point centered in the middle of the cell. Above and below this stagnation point we can observe four cell structures that are actually the cross section of two re-circulation tores. In the literature [1-5] on rotating disks, this flow topology is referred as a two cells flow structure. They are the result of the radial ejection with a central suction on both disks. The separation of both tores is marked by a strong radial jet coming from the cylinder wall to the centre. For $S=-1$ the separation is exactly in the middle plan of the cylinder. On the next picture, $S=-0.53$, the separation moves above (actually, closer to the lowest rotating disk) and only one re-circulation tore is now observable near the bottom disk. The flow at $S=-0.2$ is very similar to that of $S=-0.53$. At $S=0$, we observe a strong coherent jet orientated from the top disk to the bottom disk. A very surprising feature is the presence of a very strong depression (appearing black) at the centre of the top disk (that do not rotate).

For the co-rotating regime, the flow also seems to encompass transitions. At $S=0.2$, the strong depression on the top disk disappears, and reappears again for $S=0.35$. In this case, the vertical jet becomes much weaker. For larger values of S , the vertical jet is even not observable anymore. From $S=0.65$ to $S=1$ we observe the increase of a large depression along the vertical symmetry axe of the cylinder. For the values of $S<1$, the depression is concentrated only around the cylinder axe, while it takes the entire volume of the cylinder at $S=+1$. At $S=+1$, all the particles are localized in the mid plan and near the wall, where the flow rotation is the weakest (due to the dissipation occuring at the cylinder wall). The small white regions appearing in the middle are air bubbles introduced in the flow trough a leak in the watertight joints.

5. Discussion

5.1 Similitude laws

The torques on both disks are found to depend mostly on the rotation frequencies (figure 3). We can thus model the mean torques as :

$$\Gamma_B(f_B ; f_T) = f_B f_T H_T(S) \text{ and } \Gamma_T(f_B ; f_T) = f_B f_T H_B(S),$$

where $H_T(S) = H_B(1/S)$ (due to the inversion symmetry) is a non-dimensional function which depends only on the geometry of the system. At first order, this system does not depend on the viscosity (in the range of our measurements) whatever the frequency ratio. This observation was already reported [13] but only for $S=-1$ who ascribed this effect to an inertial stirring of the turbulence. The system actually seems to be inertial even for larger range of frequency ratios. However, if we look closer, some significant effect due to the viscosity is found on the total torque exerted on the inner wall of the cylinder (figure 4). In this case, a large amount of the total energy is dissipated on the smooth wall. For instance for $S=1$, the bulk rotates as a solid body and most of the strain, hence the dissipation is only localized on the inner smooth wall. The friction law is here similar to what is obtained in smooth plates, which depends on the viscosity. On the other hand it is very interesting to find that for the counter-rotating regime around $S=-1$ (approximately $-1.33 \leq S \leq -0.67$), dissipation occurring at the wall does not depend on viscosity. This result seems in contradiction with the friction law on smooth wall in case of turbulent boundary layer. Actually, the turbulent friction exerted on smooth flat plates [18] depends on viscosity. This dependence is related to the decrease of the turbulent boundary layer thickness as the Reynolds number increases. We can then think that the observation of a constant friction is due to a constant turbulent boundary layer thickness on the inner wall of the cylinder. If this is the case, the effect is probably

related to the strong elongationnal stress at the wall between the cells. At the moment we do not have more evidence for such effect that should deserve for further comprehension.

5.2 *The transition at $S=-0.69$*

One of the most striking transition that can be observable on the torque measurements occurs at $S=-0.69$ (or $S= -1.45$) in figure 2 and 3. This transition can be related in the flow to the transition from the one cell flow structure to a two cells flow structure. Such transition has already been reported in cases of counter-rotating smooth disks [3,4]. A two cells structure corresponds to a situation where the centre part of both disks sucks the flow. The two cells are clearly observable in figure 5(a) for $S=-1$ and correspond to the sections of two re-circulation tores. A one cell structure corresponds to a situation where the centre part of the disk having the larger frequency rotation sucks the flow, while the centre part of the other disk having a lower rotation frequency ejects the flow. Such situation is observable in figure 5(d) for $S=0$ where only one recirculation torus is present. In previous works concerning smooth disks, the transition is found to depend strongly on the Eckman number but to be independent of the aspect ratio of the experiment [3,4]. The Ekman number compares the thickness of the boundary layer on the disk to the distance between both disks. It is defined as : $Ek = \left(\frac{\delta}{H}\right)^2$. In smooth disks experiment the velocity gradient are located in the boundary layer (see figure 7) on the disk and decreases (as the Ekman number) when the Reynolds number increases. For an inertially driven flow (disks with blades), the situation is very different since the mean flow does not present any velocity gradients in the vicinity of the disks but are distributed in the bulk (see figure 7). There is in this case an effective [19] boundary layer in the bulk that does not depend on the Reynolds number which should correspond to a very large Ekman number. Dijkstra & Heijst [3] computed analytically the critical value for the transition S_c in

the case $Ek \rightarrow +\infty$ and found $S_c = -2/3$. The value is very close to ours (-0.69 compared to -0.67), it then confirms the similitude between the smooth disks flow with a large viscosity (large Ek) and the mean flow of the inertially driven turbulent flow. The reason for this similitude is the large efficiency in both cases of the momentum transport in the flow. We can notice that the critical value obtained in our experiment is slightly larger. This effect could be related to the detail of the azimuthal velocity profile that is linear in the flow produced by smooth disks at infinite Ekman number and having a tangent hyperbolic shape in our flow (see figure 7). The experiment of Ravelet [16] confirms the role of the mean flow detail since a transition at $S = -0.78$ is found with their geometry.

5.3 The torque fluctuations versus S .

In figure 3(b), the torque fluctuations present drastic changes versus the angular velocity ratio S . There are two very distinct maxima at $S = -1$ and $S = 0.06$. An third local maximum is also observable at $S = 0.23$. For the exact counter rotating regime, $S = -1$; the mean flow correspond to a stagnation point in the middle of the cell (see figure 5(a)). This type of flow is known to be very unstable [20] which then could explain the large magnitude of the fluctuations. For larger velocity ratio, the torque fluctuations have a minima for $S = -0.60$ which is close to the transition between the one and the two cells flow structures (see discussion 5.2). The torque fluctuations then increase continuously from $S = -0.6$ to $S = +0.06$ where the magnitudes of the fluctuations are comparable to those at $S = -1$. The flow instationarity here is probably related to the vortex breakdown dynamics that appear in the rotor stator configuration [21].

For larger values of S , the fluctuations decreases mostly until the co-rotating regime $S = +1$. However, a transition is observable around $S = 0.2$. This transition could be related to

the appearance of a second recirculation cell similarly to the counter-rotating regime (read discussion 5.2). Actually it is known [22] that if the cylinder is fixed, both disk should produce a suction leading to a two cell flow structure for $S=+1$. The flow should then undergo a transition between $S=0$ and $S=+1$. On our visualization, it is difficult to check this idea. The picture $S=0.2$ in figure 6 gives some indications. One can observe a strong suction due to the top disk that rotates the fastest, but also a small torus section on the bottom disk, showing that the bottom disk sucks the flow as well. This figure then suggests that the flow consist in a two cells structure at $S=0.2$.

6. Conclusion

The measurements of the torques driving the turbulent flow for this geometry provide results about the similitude laws. The flow is found to be fully inertial for any contribution of the torques (disks and smooth inner cylinder wall) for the rotation angular velocity ratio in the range $-1.33 < S < -0.67$. This range correspond to the existence of two cells in the bulk. We then believe the strong elongationnal stress at the wall to be responsible for this inertial behavior. For this range the similitude laws for the torques are then simple; whatever the Reynolds number explored, the non dimensional torque (based on the inertial stirring) only depend on S . For a given ratio S , the non dimensional torques of the bottom and the top stirrer respectively are identically equal to those obtain for the ratio $1/S$ of the top and the bottom stirrer respectively. For rotational frequency ratios outside from this range, we find the the energy injection to depend on the viscosity, mainly due the torque exerted on the inner smooth wall that behave now as a conventional turbulent friction law. However, the similitude laws discussed above are reasonably followed and a good representation of torques can be given in the range $S = [-1; +1]$. Global transitions are observed versus S , shown of by abrupt changes in

both the mean torques and the torques fluctuations. A transition occurring at $S=-0.69$ is clearly identified corresponding to the well known one to two cells transition. A similar transition is also detected in the co-rotating regime ($S>1$).

Acknowledgements

We are grateful to Arnaud Chiffaudel for his critical reading of the manuscript.

REFERENCES

- [1] P. J. Zandbergen and D. Dijkstra, Von Karman swirling flows, *Ann. Rev. Fluid Mech.* 19, {1987}465.
- [2] This theoretical problem opposed G. K. Batchelor and K. Stewartson in the 50's. Both point of views have been then unified because of the non-unicity of the solutions [3]. G. K. Batchelor, Note on a class of solutions of the Navier-Stokes equations representing steady rotationally-symmetric flow, *Quart. Journ. Mech. and Applied Math.*, 4, (1951) 29. K. Stewartson, On the flow between two rotating coaxial disks, *Proc. Cambridge Philos. Soc* 42, (1953) 333.
- [3] D. Dijkstra and G. J. F Van Heijst, The flow between two finite rotating disks enclosed by a cylinder, *J. Fluid Mech.*, 128, (1983) 123.
- [4] H. J. Lugt and H. J. Haussling, Development of flow circulation in a rotating tank, *Acta Mechanica* 18, (1973) 255.
- [5] S. Douady, Y. Couder, M.-E. Brachet, Direct observation of the intermittency of intense vorticity filaments in turbulence, *Phys. Rev. Lett.* 67, (1991) 983.
- [6] O. Cadot, S. Douady, and Y. Couder, Characterization of the low pressure filaments in a three-dimensional shear flow, *Phys. Fluids* 7(3), (1995) 630.
- [7] R. Labbé, J.-F. Pinton, S. Fauve, Power fluctuations in turbulent swirling flows, *J. Phys. II France* 6, (1996) 1099.
- [8] O. Cadot and J.H. Titon, On the relationship of the injected power between constant torque forcing constant velocity forcing of fully turbulent flow, *Physics of Fluids*, 16(6), (2004) 2140.

- [9] O. Cadot, D. Bonn & S. Douady, Turbulent drag reduction in a closed flow system : boundary layer vs. bulk effects, *Phys. Fluids* 10(2), (1998) 426.
- [10] F. Moisy, H. Willaime, J. Andersen & P. Tabeling, Passive scalar intermittency in low temperature helium flows, *Phys. Rev. Lett.* 86(21), (2001) 4827.
- [11] G. A. Voth, A. La Porta, A.M. Crawford, J. Alexander & E. Bodenschatz, Measurement of particle accelerations in fully developed turbulence, *J. Fluid Mech.* 469, (2002) 121.
- [12] F. Pétrélis, M. Bourgoïn, L. Marié, A. Chiffaudel, S. Fauve, F. Daviaud, P. Odier & J.-F. Pinton "Non linear induction in a swirling flow of liquid sodium". *Phys. Rev. Lett.* 90(17), (2003) 174501.
- [13] O. Cadot, Y. Couder, A. Daerr, S. Douady and A. Tsinober, Energy injection in closed turbulent flow : stirring through boundary-layers versus inertial stirring, *Phys. Rev. E*, 56 (1997) 427.
- [14] J. H. Titon and O. Cadot, The statistics of power injected in a closed turbulent flow : constant torque forcing vs. constant velocity forcing, *Physics of Fluids*, 15(3), (2003) 625.
- [15] L. Marié and F. Daviaud, Experimental measurement of the scale-by-scale momentum transport budget in a turbulent shear flow, *Phys. Fluid* 16(2) (2004) 457.
- [16] F. Ravelet, Bifurcation globales hydrodynamiques et magnétohydrodynamiques dans écoulement de von Karman turbulent, *PHD thesis* of Ecole Doctorale de l'Ecole Polytechnique (2005).
- [17] F. Ravelet, L. Marie, A. Chiffaudel and F. Daviaud, Multistability and Memory Effect in a Highly Turbulent Flow: Experimental Evidence for a Global Bifurcation, *Phys. Rev. Lett.* 93, (2004) 164501.
- [18] H. Schlichting, K. Gersten, *Boundary layer theory* Springer 2000.
- [19] O. Cadot, D. Bonn and S. Douady, Turbulent drag reduction in a closed flow system: boundary layer vs. Bulk effects, *Phys. Fluids* 10 (2) (1998) 426.
- [20] B. Andreotti, S. Douady and Y. Couder, An experiment on two aspects of the interaction between strain and vorticity, *J. Fluid Mech.*, 444. (2001) 151.
- [21] A. Spohn, M. Mory and E. J. Hopfinger, Experiments on vortex breakdown in a confined flow generated by a rotating disc, *J. Fluid Mech.* 370, (1998) 73.
- [22] J. A. C. Humphrey and D. Gor, Experimental observations of an unsteady detached shear layer in enclosed corotating flow, *Phys. Fluids A* 5(10) (1993) 2438.

	f_B	f_T	$S = f/f_0$	$1/S$
Run #1	$f_0 = 5.8 \text{ Hz}$	$-10.6 \text{ Hz} < f < 11.5 \text{ Hz}$	$[-1.83 ; 1.98]$	$[\dots ; -0.54] \cup [0.50 ; \dots]$
Run #2	$-10.8 \text{ Hz} < f < 10.6 \text{ Hz}$	$f_0 = 5.8 \text{ Hz}$	$[-1.86 ; 1.83]$	$[\dots ; -0.54] \cup [0.55 ; \dots]$
Run #3	$f_0 = 4.5 \text{ Hz}$	$-10.2 \text{ Hz} < f < 10.9 \text{ Hz}$	$[-2.26 ; 2.41]$	$[\dots ; -0.44] \cup [0.41 ; \dots]$

TABLE 1 : The three experimental runs #1, #2 and #3 with the corresponding ranges of the rotation frequencies for both top and bottom disks. The parameter S is the frequency ratio.

FIGURE CAPTIONS

Fig.1 : Cross section (a) of the cylindrical experimental cell. The total volume of fluid is comprised in a surface Σ that decomposed itself into three parts. A fixed part (dashed line) of surface Σ_w corresponding to the wall's cell and two rotating parts corresponding to Σ_T , the surface of the top disk and Σ_B , the surface of the bottom disk. Detail (a) of one disk with the arrangement of the six blades.

Fig.2 : Torque measurements versus the rotation frequency ratio S . The non dimensionnal time averaged torques (a) $\langle \Gamma_T \rangle / f_B^2$ and $\langle \Gamma_B \rangle / f_B^2$ are displayed for two different fixed rotation frequency of the bottom disk (run #1 and run #3, see table 1). In (a), $\langle \Gamma_B \rangle / f_T^2$ and $\langle \Gamma_T \rangle / f_T^2$ measured in run #2 are respectively the symmetric (see eq. 6) of $\langle \Gamma_T \rangle / f_B^2$ and $\langle \Gamma_B \rangle / f_B^2$ measured in run#1. The non dimensionnal torque fluctuations (b), $\delta \Gamma_T / f_B^2$ and $\delta \Gamma_B / f_B^2$ are displayed for two different fixed rotation frequency of the bottom disk (run #1 and run #3, see table 1). In (b), $\delta \Gamma_B / f_T^2$ and $\delta \Gamma_T / f_T^2$ measured in run #2 are respectively the symmetric (see eq. 6) of $\delta \Gamma_T / f_B^2$ and $\delta \Gamma_B / f_B^2$ measured in run#1.

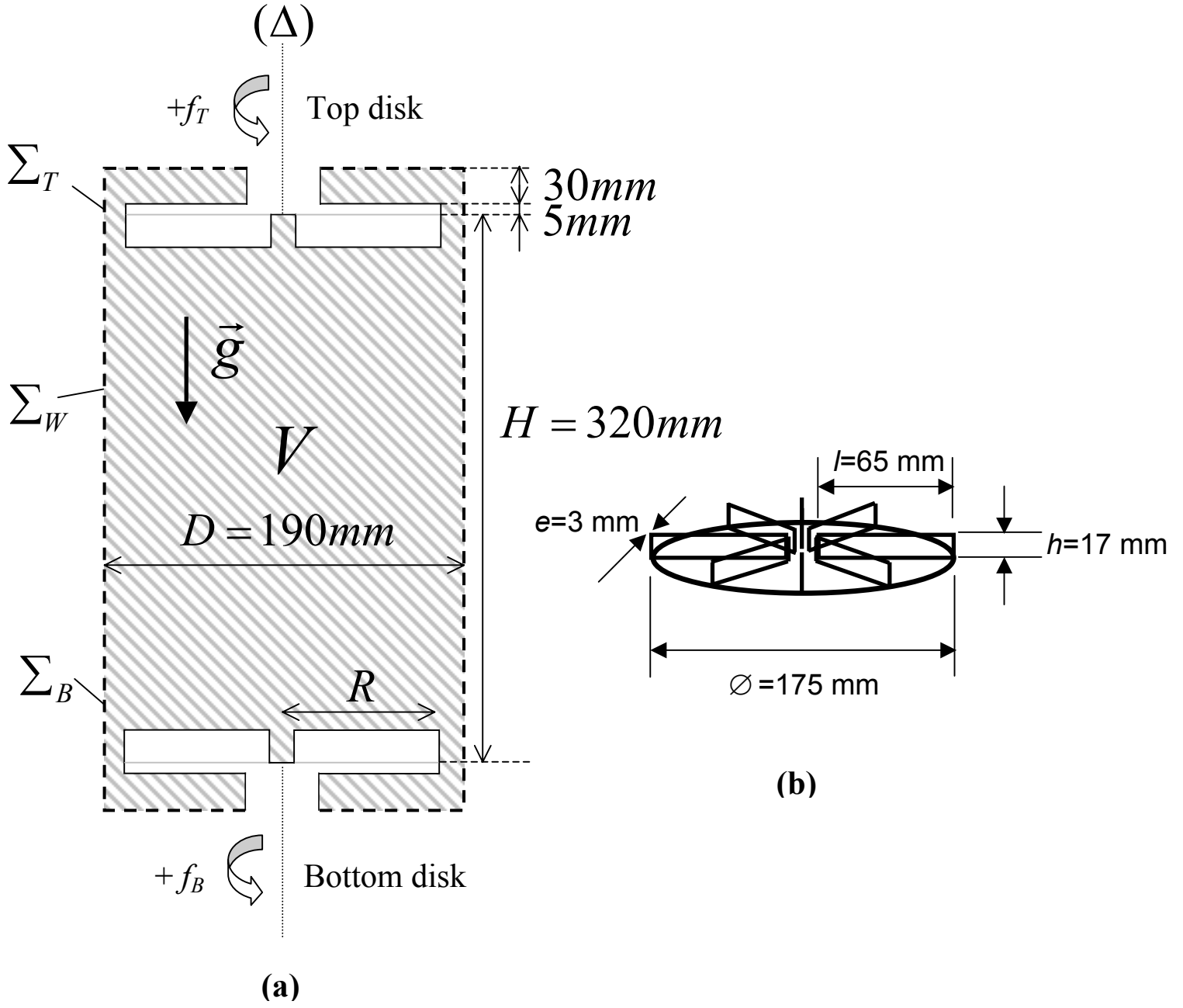
Fig.3 : Similitude laws checking for the non dimensionnal averaged torques (a) and the non dimensionnal fluctuation torques (b) for run #1 versus $S \in [-1,1]$. The measurements shown of by crosses are deduced from the torque measurements for $S \leq -1$ and $S \geq 1$. For this representation the two symetries of eq. 5 and eq.6 are needed.

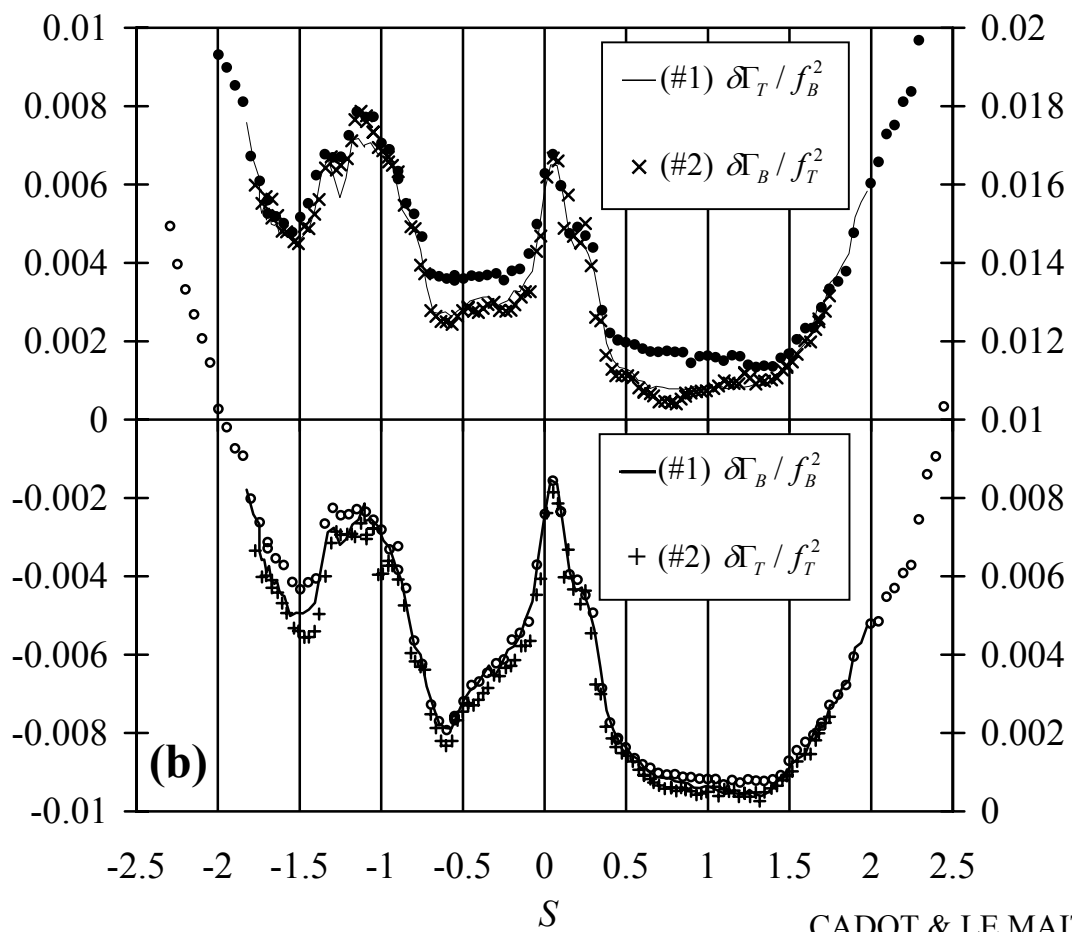
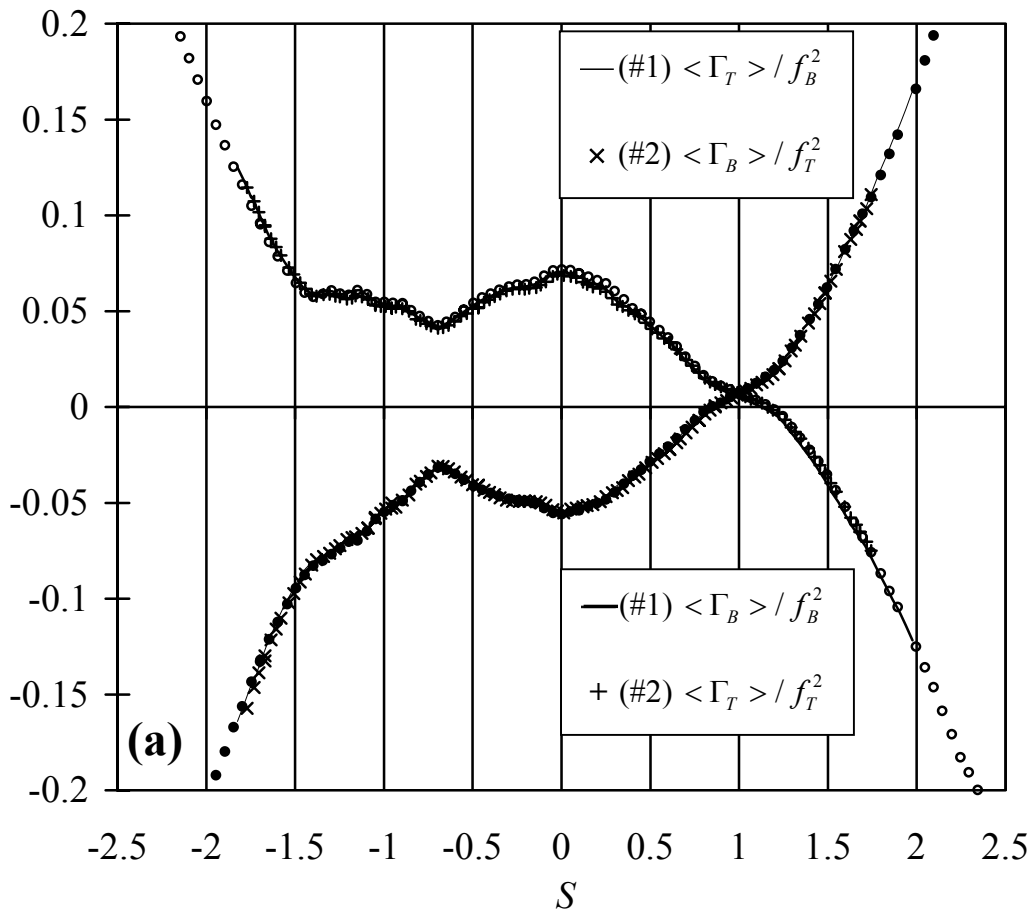
Fig.4 : Non dimensional average torque over the inner smooth wall versus $S \in [-1,1]$ for run #1 and #3. The measurements shown of by crosses are deduced from the for $S \leq -1$ and $S \geq 1$. For this representation the two symmetries of eq. 5 and eq.6 are needed.

Fig.5 : Flow visualization of the counter-rotating regime, $S \leq 0$. The bottom disk's rotation frequency is set to 4.5 Hz.

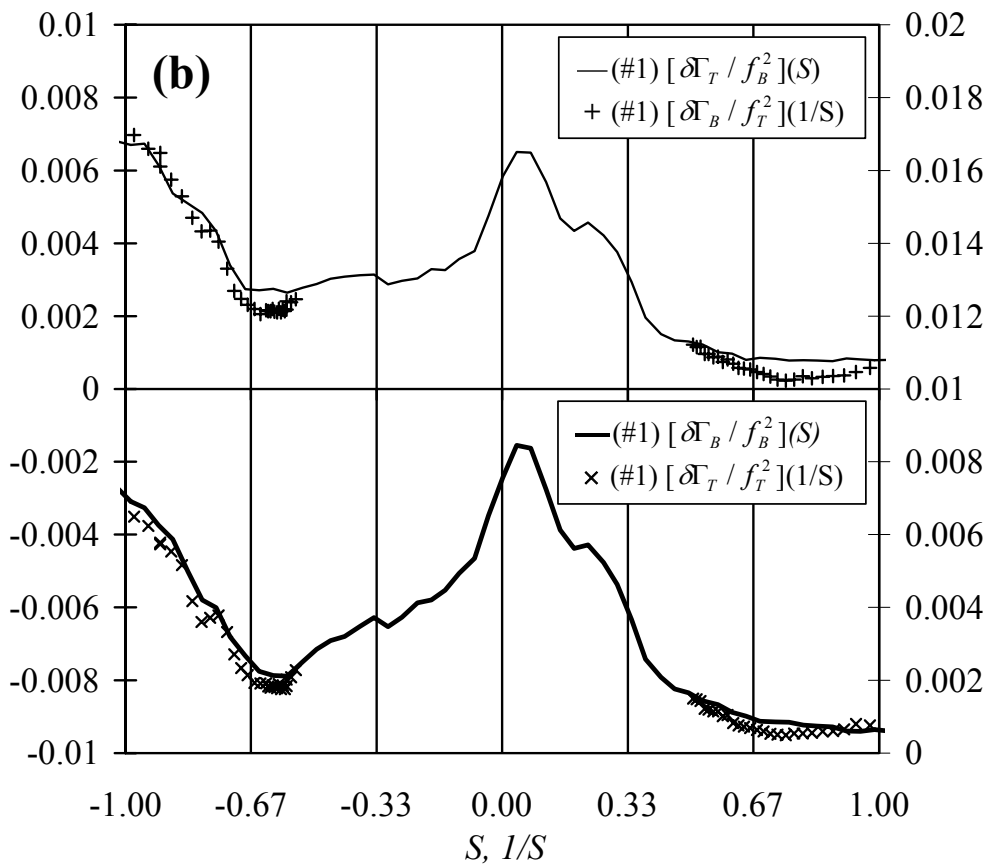
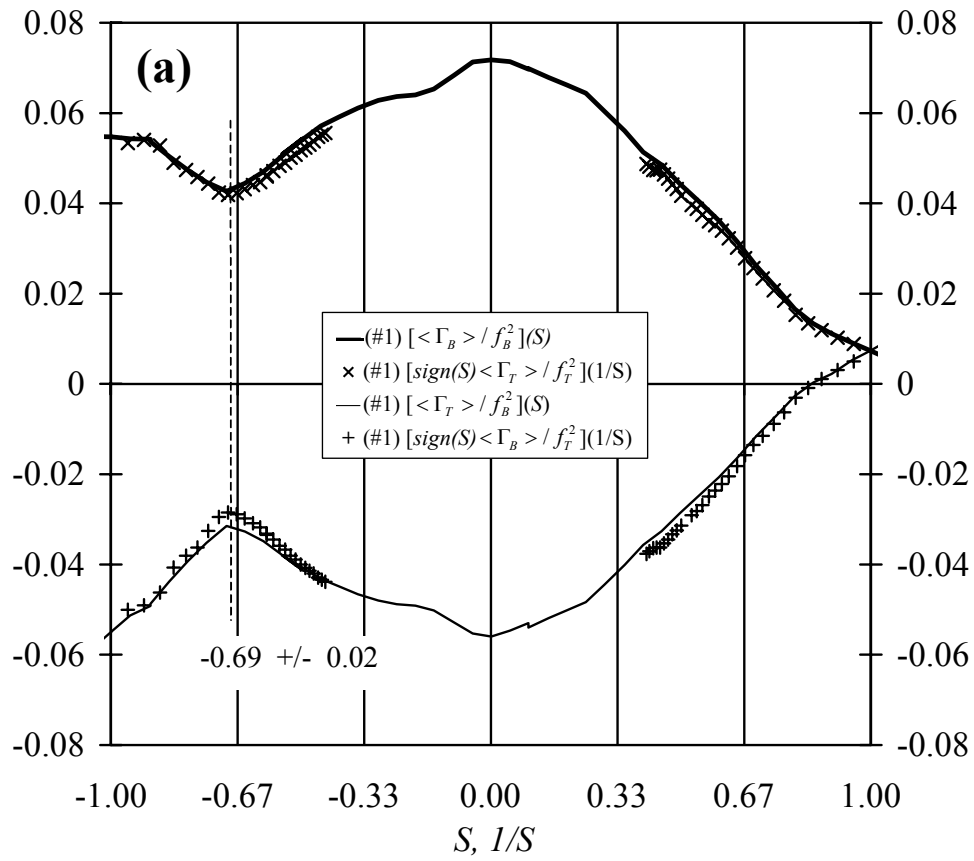
Fig.6 : Flow visualization of the co-rotating regime $S > 0$. The bottom disk's rotation frequency is set to 4.5 Hz.

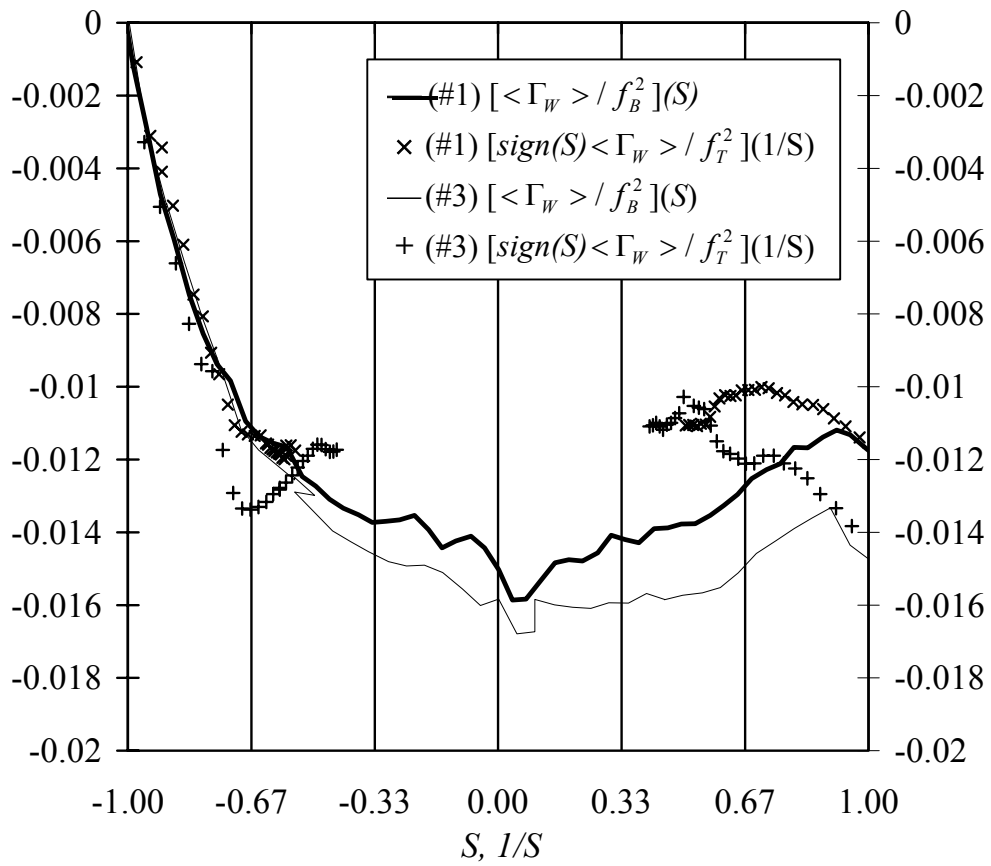
Fig.7 : Laser doppler velocimetry measurements of the orthoradial velocity profile $v_\theta(2z/H)$ along a vertical axis located at $R_m = 0.7 R$. $z=0$ defines the middle plan of the cylindrical cell and H is the distance separating both disks. The error bars correspond the *rms* values of the velocity. When the disks are equipped with blade, the velocity profile corresponds very schematically to the dashed thin line, that joins the boundary condition at the disks without any velocity gradient. In contrast, with smooth disks, the velocity profile should join the boundary condition at the disks through a thin viscous boundary layer as depicted by the dashed thick line.



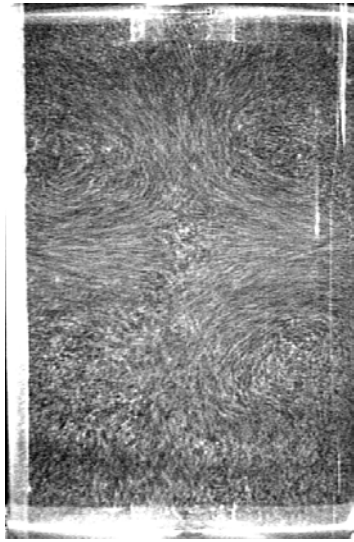


CADOT & LE MAITRE, FIG.2

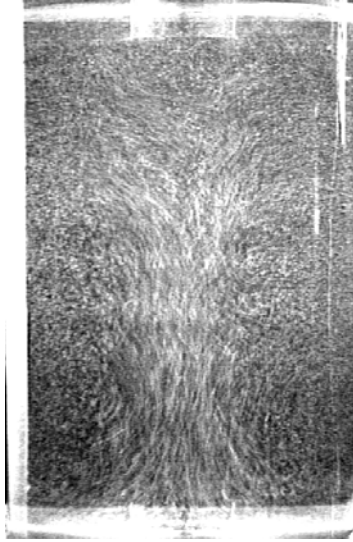




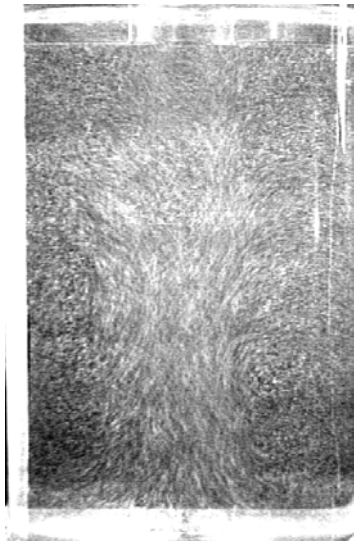
$S = -1$



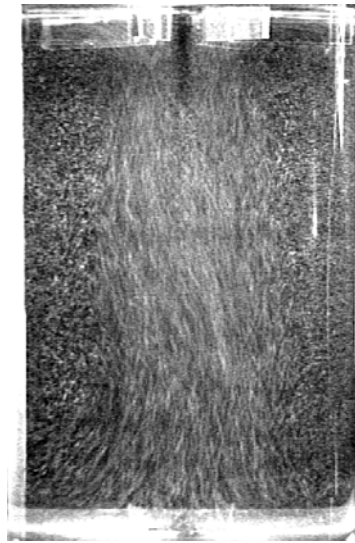
$S = -0.53$



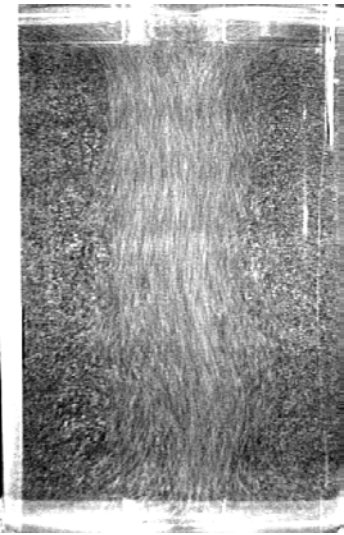
$S = -0.2$



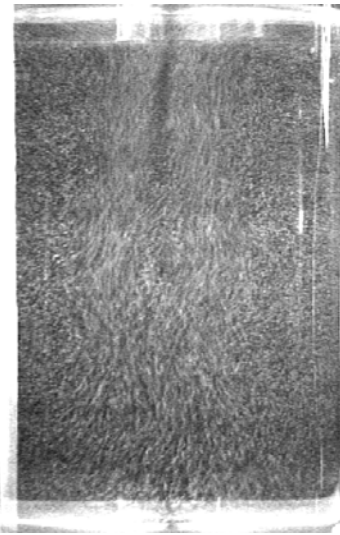
$S = 0$



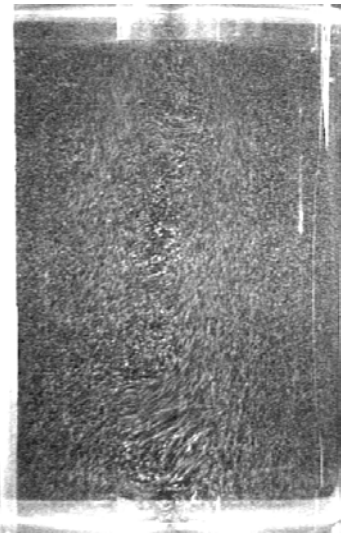
$S = +0.$



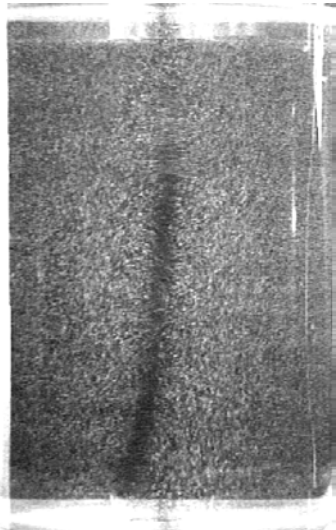
$S = +0.35$



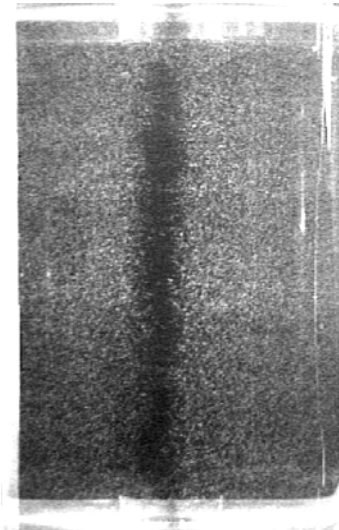
$S = +0.53$



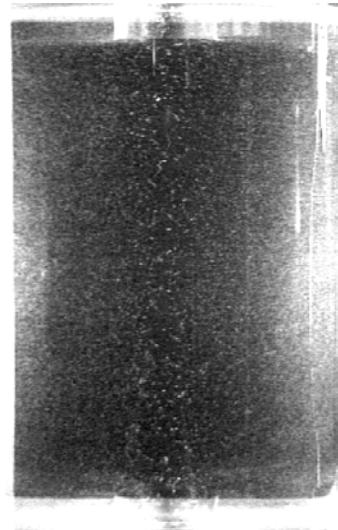
$S = +0.65$

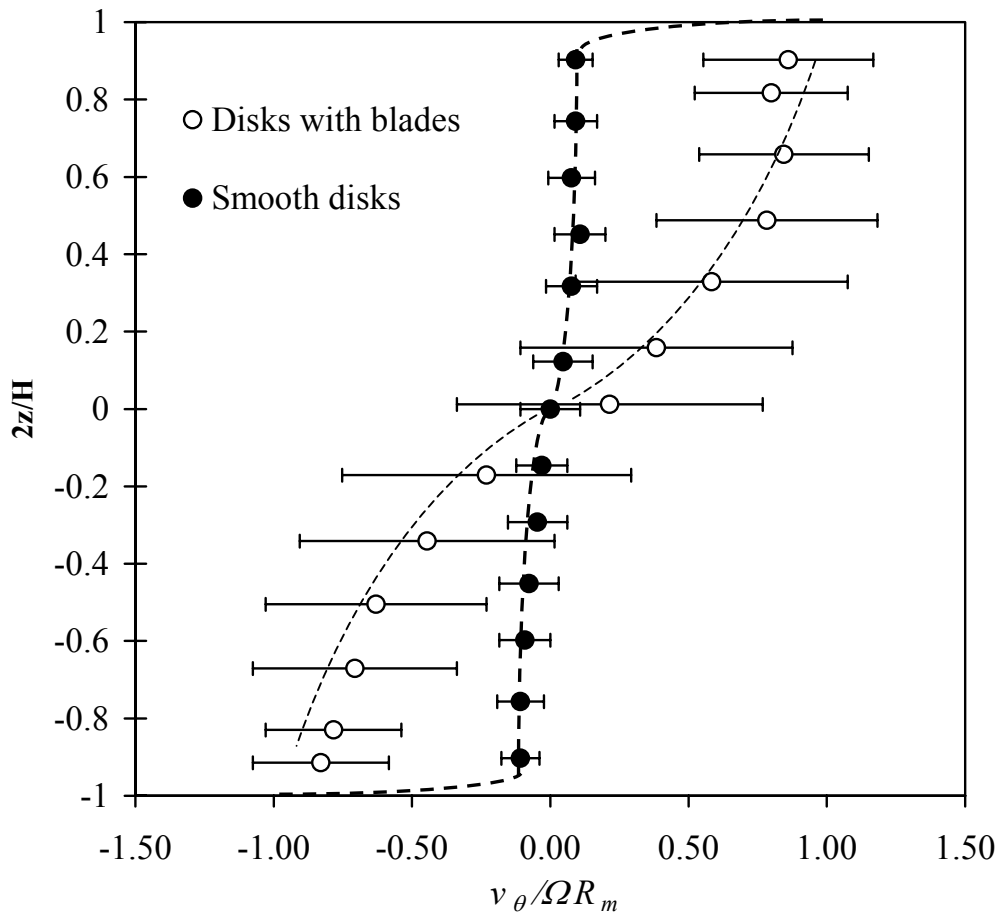


$S = +0.75$



$S = +1$





Cadot & Le Maître, FIG.7